

# **Deciphering the co-formation of layered two-dimensional hybrid $\text{CdCl}_2(\text{hexylamine})_2$ and CdS nanocrystals**

*A thesis submitted to*

**Indian Institute of Science Education and Research, Pune**

*in partial fulfilment of the requirements for the*

**M.Sc. Chemistry Degree Programme**



*by*

**Pavithra Parthiban**

20226213

*under the supervision of*

**Prof. Angshuman Nag**

Associate Professor, Department of Chemistry

Indian Institute of Science Education and Research, Pune

Dr. Homi Bhabha Road, Pashan

Pune – 411008.

# Certificate

---

This is to certify that this dissertation entitled “**Deciphering the co-formation of layered two-dimensional hybrid  $\text{CdCl}_2(\text{hexylamine})_2$  and CdS nanocrystals**” towards the partial fulfilment of the M.Sc Chemistry degree programme at the Indian Institute of Science Education and Research (IISER), Pune represents study/work carried out by Pavithra Parthiban at IISER Pune under the supervision of Prof. Angshuman Nag, Associate Professor, Department of Chemistry during the academic year 2023-24.



**Date:** 10-Apr-2024

**Pavithra Parthiban**



**Prof Angshuman Nag**  
**(Research Supervisor)**

---

*This thesis is dedicated to my family  
and the people who've become family.*


## Declaration

---

I hereby declare that the matter embodied in the report entitled “**Deciphering the co-formation of layered two-dimensional hybrid  $\text{CdCl}_2(\text{hexylamine})_2$  and CdS nanocrystals**” are the results of the work carried out by me at the Department of Chemistry, Indian Institute of Science Education and Research, Pune, under the supervision of Prof. Angshuman Nag and the same has not been submitted elsewhere for any other degree.

**Date:** 10-Apr-2024

  
**Pavithra Parthiban**

  
**Prof Angshuman Nag**  
(Research Supervisor)

# Acknowledgement

---

The theory of chaos suggests that even minor changes cause significant effects in a dynamic systems highly sensitive to initial conditions. Echoing the concept that a butterfly's flutter in one place can set off a hurricane on the other side of the globe, my master's thesis project at IISER Pune is a culmination of seemingly insignificant actions of many individuals creating ripple effects that resonate through time. Each of these individuals deserves my heartfelt gratitude and admiration. Among them, my thesis supervisor, **Prof Angshuman Nag**, played the most pivotal role, whose guidance was paramount throughout my tenure. I must specifically thank and appreciate him for creating a welcoming group with wonderful people who are always willing to collaborate, brainstorm or help out a fellow lab member. His visible enthusiasm for science and his commitment towards teaching has been a source of inspiration for all my academic pursuits in the past one year.

Next, I thank **Dr Pramod Pillai** for his guidance as the expert member for this master's thesis project and his valuable insights during the mid-year presentation. I am immensely grateful to **Prof Boomi Shankar** and Rishu Kumar Pandey for single crystal structure refinement. I am thankful to **IISER Pune** and especially the **Department of Chemistry** for providing the infrastructure for carrying out my research work. I am grateful to all the technical and non-technical staff of the department as well.

A special thanks to Urmila Makhija for being a great mentor and an even better friend since my early days in the lab. Thanks to all my lab members who supported me during this journey in both the professional and personal realms, especially Parikshit Rajput and Srijita Banerjee. Both of them have gone above and beyond to help me every time I was in need of guidance. Thanks to Sajid Saikia for his invaluable contributions in the lab as a scientist during day and as a singer at night. Also, I would always cherish the time I spent with Manmayuri Sarma, Ajinkya Shingote and Vijay Tripathi. I thank them for bringing contagious joy and cheer to an otherwise intense environment. Being new to the laboratory and world the scientific research, the past year would've been much harder without the encouragement and inputs from all of these people – Dr Aparna Shinde, Dr Habibul Arfin, Barnali Mondal, Taniya Dutta, and Animesh Ghosh.

My genuine appreciation goes out to Dev, Sundara and Vedhanth for making tough days at IISER Pune a bit easier with their sense of humour. Finally, I am truly fortunate to have the constant moral and emotional support from my parents and sister. Thank you, all three!

# Table of Contents

---

## Abstract

<b>1. Chapter 1</b>	<b>9</b>
1.1 Introduction	9
1.2 Synthesis	12
1.2.1 Chemicals	
1.2.2 Methodology	
1.3 Instrumentation	12
1.3.1 Powder X-Ray Diffraction	
1.3.2 Field Emission Scanning Electron Microscopy	
1.3.3 Energy Dispersive X-Ray Spectroscopy	
1.3.4 High Resolution Transmission Electron Microscopy	
1.3.5 Diffuse Reflectance Spectroscopy	
1.3.6 Steady-state Photoluminescence	
1.3.7 Time-Correlated Single Photon Counting	
<b>2. Chapter 2</b>	<b>15</b>
2.1 Structural Characterization	15
2.2 Optical Characterization	18
<b>3. Chapter 3</b>	
3.1 Summary and Outlook	25

## Bibliography

## List of Figures

---

**Figure 1.1.** A schematic showing dielectric confinement in two dimensional organic-inorganic materials.

**Figure 1.2.** A schematic showing correlation between dimensionality change and bandgap of material.

**Figure 1.3.** Schematic showing synthesis procedure of hybrid transition-metal chalcogenide.

**Figure 2.1.** Comparison of PXRD pattern of product(s) with precursors.

**Figure 2.2.** FESEM images showing layered morphology of crystals.

**Figure 2.3.** Structure of  $\text{CdCl}_2(\text{ha})_2$  at 100K and comparison with simulated PXRD pattern.

**Figure 2.4.** **a)** Difference in absorbance in presence and absence of sulfur and **b)** PXRD indicating presence of CdS nanoparticles.

**Figure 2.5.** HRTEM analysis of CdS nanoparticles.

**Figure 2.6.** **a)** Absorption spectra showing optical bandgap of 2.64 eV **b)** Photoluminescence spectra on excitation with 375 nm laser.

**Figure 2.7.** **a)** Photoluminescence decay of 474 nm peak shown along with Instrument Response Function (IRF) **b)** Photoluminescence decay of 600 nm peak shown along with IRF ( $\lambda_{\text{ex}} = 375 \text{ nm}$  laser)

**Figure 2.8.** Photoluminescence spectra measured at different temperatures between 300K to 7K.

**Figure 2.9.** **a)** Plot showing systematic increase in integrated photoluminescence intensity with decrease in temperature **b)** Contributions of the excitonic and trap state emission to in overall integrated intensity.

**Figure 2.10.** Increase in photoluminescence decay lifetimes at lower temperatures due to reduced number of non-radiative channels.

---

**Figure 2.11. a)** Plot showing logarithmic increase in excitonic intensity with reducing temperature **b)** Temperature dependence of FWHM of excitonic emission.

**Figure 2.12. a)** Plot showing logarithmic increase in excitonic intensity with reducing temperature **b)** Temperature dependence of FWHM of excitonic emission.

**Figure 2.13. a)** Decrease in excitonic emission intensity relative to broad emission band from 7K to 155K. **b)** Relative intensity of excitonic emission increasing with respect to broad emission band from 180K to room temperature.

**Figure 2.14.** Schematic showing exciton trapping and de-trapping mechanism indicating difference in energy barrier between the two processes



## Abstract

---

While conventional quantum dots like CdS and ZnSe exhibit remarkable optical properties, their limitations in charge transport and size homogeneity pose challenges in device applications. Two-dimensional (2D) organic-inorganic hybrid derivatives offer a promising solution by enabling charge mobility in two dimensions while maintaining bandgap tunability and uniformity in size. Thus, the objective of this work is to synthesize one such 2D derivative of a IIB-VIA semiconductor – Cd<sub>2</sub>S<sub>2</sub>(hexylamine) and investigate the temperature-dependence of luminescent properties. However, structural and optical characterization following syntheses revealed that a 2D hybrid compound CdCl<sub>2</sub>(hexylamine)<sub>2</sub> forms along with CdS nanoparticles. Further, optical studies indicate the formation of excitons in the system originating from the CdS nanocrystals. The variation in luminescent behaviour of these excitons is investigated at different temperatures below 300K.

The phenomenon of semiconductor luminescence has fascinated physicists, chemists and engineers alike for the past few decades, owing to the versatility in its range of applications from Light Emitting Diodes (LEDs) and photocatalysts to quantum computing with excitonic Bose-Einstein condensates.<sup>1–5</sup> Especially since the first works of quantum dots in the 1980s, research on reduced dimensional semiconductors has increased exponentially, and the recent Nobel Prize in Chemistry serves as an evidence to this fact.<sup>6–8</sup> Reducing the dimensionality of semiconductors through dielectric and/or quantum confinement paves the way for precisely tuning the optical, electronic and magnetic properties of the material.

The role of organic molecules and ions in dimensionality reduction is significant in systems like ligand-capped nanocrystals, inorganic-organic perovskites, hybrid transition-metal chalcogenides etc.<sup>9</sup> Through subtle variations in composition, this class of materials offers an exciting playground to incorporate and modulate properties like bandgap tunability, chirality and moisture stability.<sup>10</sup> Further, the freedom of choice in incorporation of the organic component offers a rich platform to design materials with novel properties such as second- order optical nonlinearity, ferroelectricity, and chiral-induced spin selectivity (CISS Effect) to name a few.<sup>11–13</sup> When one talks about quantum confined luminescent semiconductors, a great deal of attention has been given to investigating the excellent optical properties of quantum dots, especially II-VI compositions such as CdS, CdTe, ZnSe etc. Although this class of quantum dots exhibit outstanding bandgap tunability and color purity, these do not possess electroluminescence and charge transport properties due to the dielectric confinement in all directions as a result of using organic capping ligands. Charge transport and mobility become a source of concern while designing optoelectronic devices. Moreover, achieving homogeneity in size has always been a challenge in the synthesis of nanoparticles. Two-dimensional (2D) materials appear to strike an interesting balance by allowing movement of charges in two directions, while retaining the tunability of properties that comes with the quantum confinement effect. Further, these systems have uniformly-sized nanocomponents arranged in a periodic lattice, which solves the problem of heterogeneity in size.

While organic-inorganic two-dimensional materials like 2D hybrid halide perovskites have been in the spotlight for quite a while now, 2D derivatives of IIB-VIA semiconductors have not been as extensively studied. Jing Li et al. first reported this type of materials by incorporating neutral organic amines into the typical inorganic network structure, known as inorganic-organic hybrid transition metal chalcogenides.<sup>14</sup> One can imagine the structure of this class of compounds as a slice of an inorganic semiconducting layer sandwiched between organic spacers, giving rise to a quantum well structure (Figure 1.1).

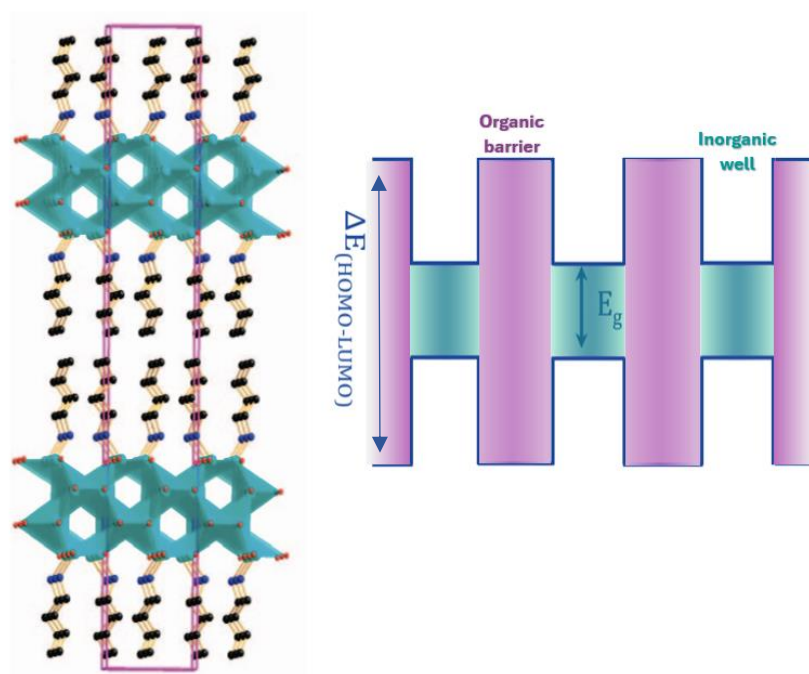


**Figure 1.1.** A schematic showing dielectric confinement in two dimensional organic-inorganic materials. The crystal of structure of Cd<sub>2</sub>S<sub>2</sub>(ba) is shown for representative purposes, originally published by Wooseok Ki and Jing Li, *J. Am. Chem. Soc.* **2008**, 130, 26, 8114–811.

Later, it was demonstrated that it was possible to further tune the dimensionality of this hybrid transition-metal chalcogenides from one-dimensional chains to three dimensional networks through facile solution-processable methods (Figure 1.2).<sup>15–18</sup> Owing to the presence of emissive mid-gap states in these systems, direct white-light emission has been observed in room temperature in ternary compositions such as Zn<sub>1.7</sub>Cd<sub>0.3</sub>S<sub>2</sub>(octylamine), with about 25% fluorescence quantum yield.<sup>19,20</sup>

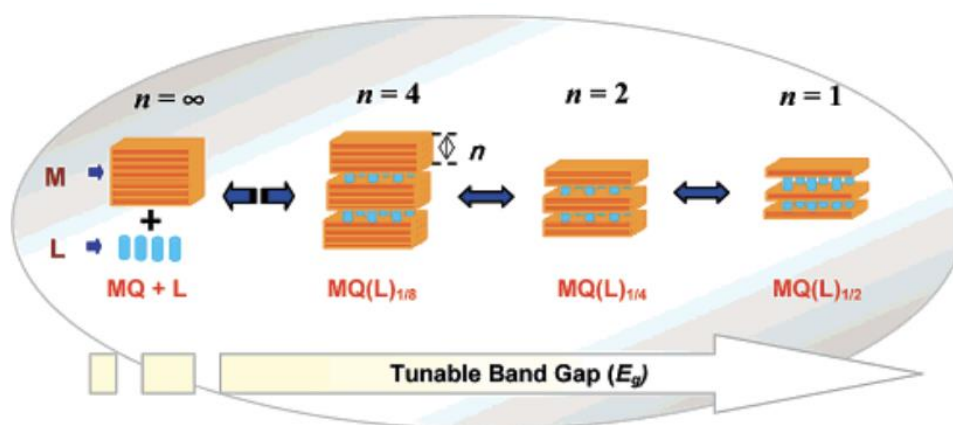


**Figure 1.2.** A schematic showing correlation between dimensionality change and bandgap of material, published by Xiaoying Huang and Jing Li, *J. Am. Chem. Soc.* **2007**, 129, 3157–3162.

Studies also show facile doping of  $\text{Te}^{2-}$ ,  $\text{Mn}^{2+}$  and  $\text{Zn}^{2+}$  ions as well as mixed chalcogenide compositions to tune and enhance emissive properties in these materials.<sup>21,22</sup> More recently, the role of organic amine spacer on dimensional tuning, thermal stability, thermal conductivity and enhancing luminescence intensity have been explored.<sup>23,24</sup> Thus, these hybrid II-VI semiconductors have high potential for applications in efficient optoelectronic devices. However, the effect of temperature on the luminescence properties is yet to be investigated in this class of compounds. So, the objective of this work is to study the temperature dependent behavior of excitons in this material.

## 1.2.1 Chemicals

Cadmium(II) Chloride (TCI Chemicals, >98.0% purity), Sulfur (Sigma Aldrich, flakes,  $\geq 99.99\%$  trace metals basis), Hexylamine (TCI Chemicals, >99.0% purity). All chemicals were used without further purification.

## 1.2.2 Methodology

The protocol for the synthesis of  $\text{Cd}_2\text{S}_2(\text{hexylamine})$  was modified based on the method developed by Jing Li *et al.*<sup>14</sup> The solid reactants Sulfur (0.5 mmol, 16 mg) and Cadmium Chloride (1 mmol, 91.7 mg) were dissolved in 3ml of hexylamine (acting as solvent as well as reagent) in a round-bottom flask while purging with  $\text{N}_2$ . The precursors dissolve completely on heating at  $120^\circ\text{C}$ . The temperature was maintained for about 30 minutes and the setup was left to cool naturally in a sand bath. A yellow colored precipitate is observed as the reaction mixture cools below  $90^\circ\text{C}$ . The solid precipitate was washed with absolute ethanol three times followed by washing with acetone. The collected precipitate was dried by applying vacuum for 2 hours and was stored in an Eppendorf in a desiccator.

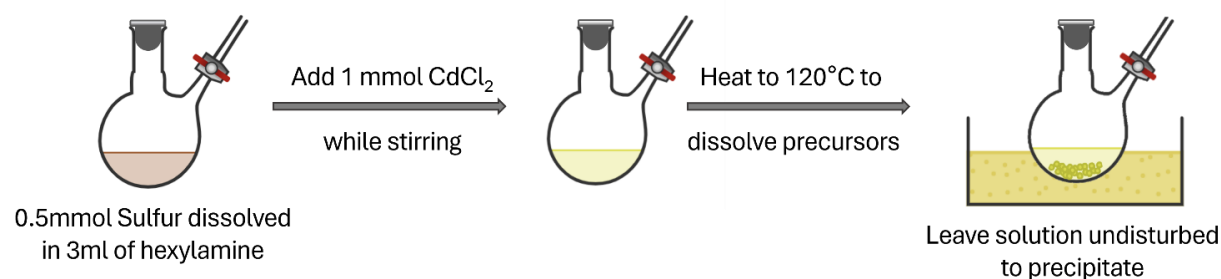


**Figure 1.3.** Schematic showing synthesis procedure of hybrid transition-metal chalcogenide.

## Instrumentation

### 1.3.1 Powder X-Ray Diffraction

Powder X-ray diffraction (PXRD) patterns were recorded using a Bruker D8 Advance X-ray diffractometer in Bragg-Brentano geometry equipped with  $\text{Cu K}\alpha$  ( $1.54 \text{ \AA}$ ) radiation. Samples were finely ground using mortar and pestle and were mounted on a glass slide for the measurements.

PXRD is a technique routinely used for the structural identification crystalline solids. It works on the principle that a distinct diffraction pattern is obtained when the wavelength of radiation is comparable to that of the atom spacings in a crystalline material. A beam of X-ray will only be diffracted when it impinges upon a set of planes in a crystal that satisfies the conditions defined by the Bragg equation:

$$n\lambda = 2d_{hkl} \cdot \sin\theta$$

where  $n$  is an integer which represents the order of the diffracted beam,  $\lambda$  is the wavelength of radiation,  $d_{hkl}$  is the distance of interplanar spacing, and  $\theta$  is the Bragg angle. The angle formed between the diffracted and incident beam is  $2\theta$ . While the Bragg equation does not give any information regarding the intensities of the diffracted beams, it clearly indicates that a plane of atoms will only diffract the radiation only when the incidence angle is  $\sin^{-1}(n\lambda/2d_{hkl})$ .

### **1.3.2 Field Emission Scanning Electron Microscope**

The FEI Nova NanoSEM 450 instrument was used for imaging, operating at 15kV. Field Emission Scanning Electron Microscope (FESEM) is widely used to visualize surface morphology, shape and structure of samples with sizes smaller than the resolving limit of an optical microscope. It uses a beam of electrons produced by a field emission source to image substances typically with a spatial resolution of upto 1.5 nanometres. A primary narrow beam of electrons, which is focussed and deflected by electronic lenses bombards the sample and the angle and velocity of the secondary electrons emitted corresponds to the surface topography of the sample.

### **1.3.3 Energy Dispersive X-Ray Spectroscopy**

The Energy Dispersive X-Ray Spectroscopy (EDS) elemental analysis and elemental mapping measurements were done in Bruker XFlash 6130 instrument, operating at 123eV for Mn K $\alpha$ . The principle of functioning of EDS is that a beam of high energy electromagnetic radiation (X-ray) is focused on the sample which ejects the core electrons of the elements present. The electrons in higher energy levels fill in the holes created and further releases energy as it relaxes, which has a direct correlation to the element's atomic number in accordance to Moseley's law.

### **1.3.4 High-Resolution Transmission Electron Microscopy**

High - Resolution Transmission Electron Microscopy (HRTEM) enables direct visualization of individual atoms and crystal lattice arrangements by allowing for resolution upto 0.5nm. The position of lattice fringes seen in the HRTEM image is directly correlated with atomic planes in the lattice. The lattice fringes arise from interference of two or more diffracted beams from a crystalline material.

### **1.3.5 Diffuse Reflectance Spectroscopy**

Diffuse Reflectance Spectra (DRS) of microcrystalline powder were collected in the region 200nm–800nm using a Shimadzu UV-3600 plus UV-VIS-NIR spectrophotometer. The reflectance spectra were converted to absorbance by using Kubelka-Munk transformation given by the equation:

$$F(R) = \alpha/s = \frac{(1 - R)^2}{2R}$$

where  $R$  is the reflectance,  $\alpha$  is the absorbance and  $s$  is the scattering co-efficient.

### **1.3.6 Steady-state Photoluminescence**

The steady-state photoluminescence (PL) spectra were recorded using Edinburg Instruments' FLS 980 spectrometer. A spectrometer typically measures the intensity of emitted light as a function of wavelength by using a diffraction grating which disperses the light spreading different wavelengths toward different angles.

Photoluminescence involves absorption of electromagnetic radiation by a substance leading to excitation of electrons to higher energy states and concomitant relaxation to the ground state accompanied by the emission of photon. A PL analysis is often used a probe to establish connections between electronic structure and linear optical properties of a material.

### **1.3.7 Time-Correlated Single Photon Counting (TCSPC)**

The photoluminescence decay was measured using Edinburgh Instruments' FLS-980 spectrofluorometer, with a pulsed picosecond diode laser of 405 nm as excitation source. TCSPC measures the time between an excitation pulse and a single emitted photon to quantify the photoluminescence lifetimes. The arrival times of photons are collected over a range and sorted chronologically to show the statistical intensity at any specific time. The Instrument Response Function (IRF) reflects the detection limit as it represents the shortest decay lifetime that can be resolved. Hence, the influence of IRF on the decay function must be accounted while measuring very short PL decay lifetimes.



A complete understanding of the crystal structure of a material is required to predict as well as correlate their optical and electronic properties. Establishing these structure-property relationships are key to design and synthesis of novel materials with desired properties. In this project, our objective was to synthesize a hybrid transition metal chalcogenide  $\text{Cd}_2\text{S}_2(\text{hexylamine})$ . This class of materials tend to form single crystals of sizes that are too small to be analysed using a Single Crystal X-Ray Diffractometer, PXRD becomes an important tool to characterize and derive the crystal structure.

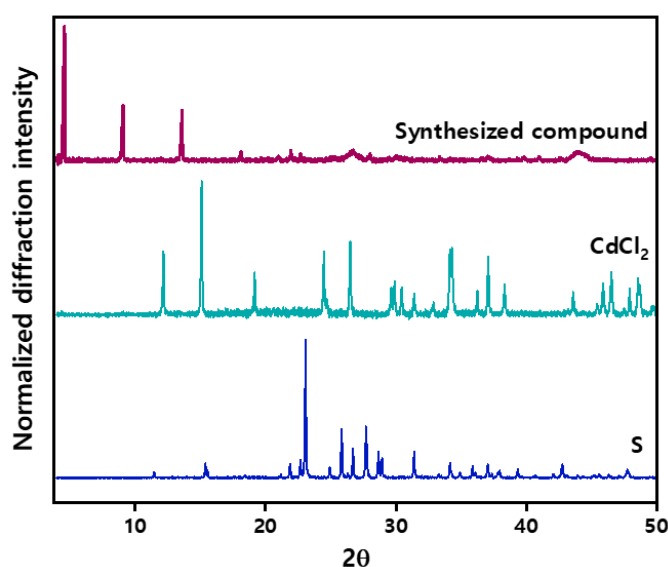


**Figure 2.1.** Comparison of PXRD pattern of product(s) with precursors

The PXRD of the synthesized compound is compared with the precursors to ensure progress of the reaction and to detect the unreacted crystalline precursors if present. The diffraction pattern (Figure 2.1) of the powdered sample shows characteristic periodicity in the first few peaks at lower angles. This suggests that the crystal has a tendency to orient itself along one of the planes predominantly, which usually occurs with crystals with layered morphology. The first peak is observed at  $2\theta = 4.59^\circ$ , indicating an interplanar separation (d-spacing) of 19.2 Å and a d-spacing of 9.71 Å and 6.51 Å is calculated for the second and third peak respectively. These values correspond to about half and one-third of the first peak indicating these are parallel planes possibly with contribution from the inorganic sheets. In case of organic-inorganic hybrid structures, the diffraction peaks with high intensities have major contribution from inorganic elements with a relatively high structure factor compared to elements like carbon, nitrogen and hydrogen.

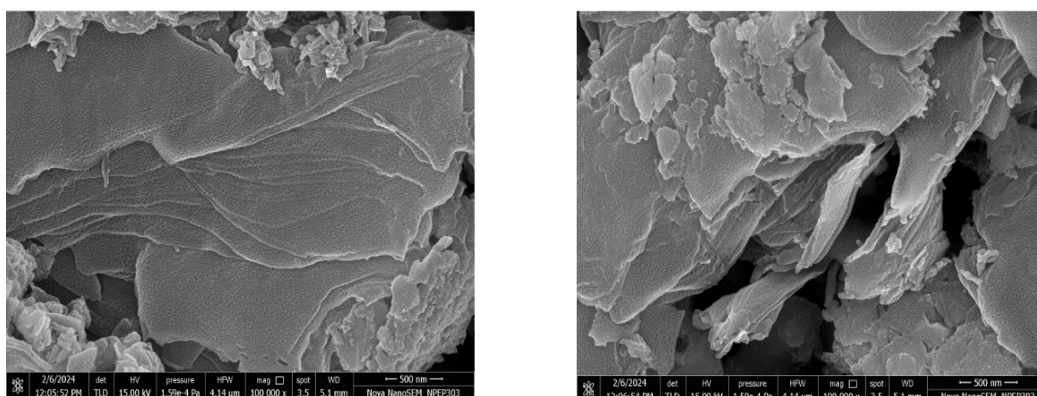


**Figure 2.2.** FESEM images showing layered morphology of crystals

To determine the macroscopic morphology of the crystals and to detect the composition of elements in the sample, FESEM imaging was done (Figure 2.2). It was observed that the crystals had a layered morphology, with sheets appearing to be stacked on top of one another, which explains the strong orientation effect seen in the PXRD pattern.

However, The EDS analysis revealed that the element Sulfur was present in negligible quantity and the ratio of Cd:Cl is found to be 1:2. Following this observation that the layered material does not have sulfur in the structure, synthesis of crystals was done using the same protocol, but in the absence of the sulfur precursor. We hypothesized a new type of cadmium chloride hybrid structure had been synthesized. We confirmed that this was indeed the case and this crystalline compound was found to be  $\text{CdCl}_2(\text{NC}_6\text{H}_{15})_2$  using SCXRD (Figure 2.3), which is an organic-inorganic hybrid halide compound. The high intensity diffraction peaks observed in lower angles which we were earlier expecting to be from  $\text{Cd}_2\text{S}_2(\text{NC}_6\text{H}_{15})$  are seen to originate from  $\text{CdCl}_2(\text{NC}_6\text{H}_{15})_2$  and it confirms that the layered hybrid Cadmium Sulfide (hexylamine) compound has not been synthesized.

Element	Atomic %	Atomic ratio	Formula (approximated)
Cd	7.94	1	1
Cl	14.9	1.9	2
S	0.29	0.03	~0

**Table 2.1.** Elemental Analysis showing measured atomic percentage and formula deduced.

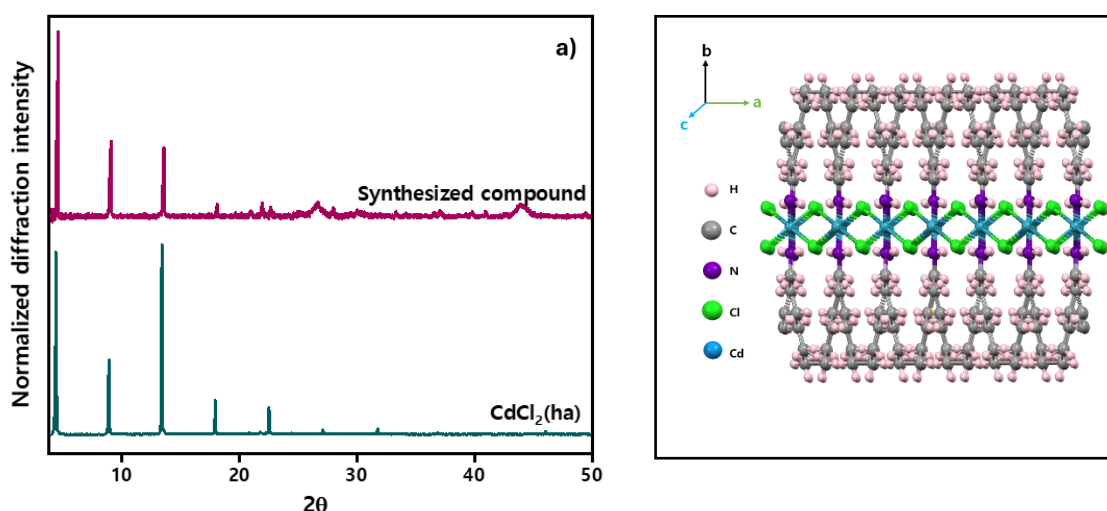


**Figure 2.3.** Structure of  $\text{CdCl}_2(\text{ha})_2$  at 100K and comparison with simulated PXRD pattern.

From the previous studies, it is evident that the major product formed was  $\text{CdCl}_2(\text{ha})_2$  (Figure 2.3). However, the optical absorption and photoluminescence properties of this compound -  $\text{CdCl}_2(\text{NC}_6\text{H}_{15})_2$  was very different from the optical properties in the presence of elemental sulfur in the reaction mixture (Figure 2.4a). Further analysis of PXRD and DRS shows that there might possibly be CdS nanoparticles formed in a small amount along with the major product in the presence of sulfur in the reaction mixture. This inference is derived based on the drastic change in the bandgap of the compound and is supported by the presence of broad peaks in PXRD matching with CdS diffraction pattern reference (Figure 2.4b).

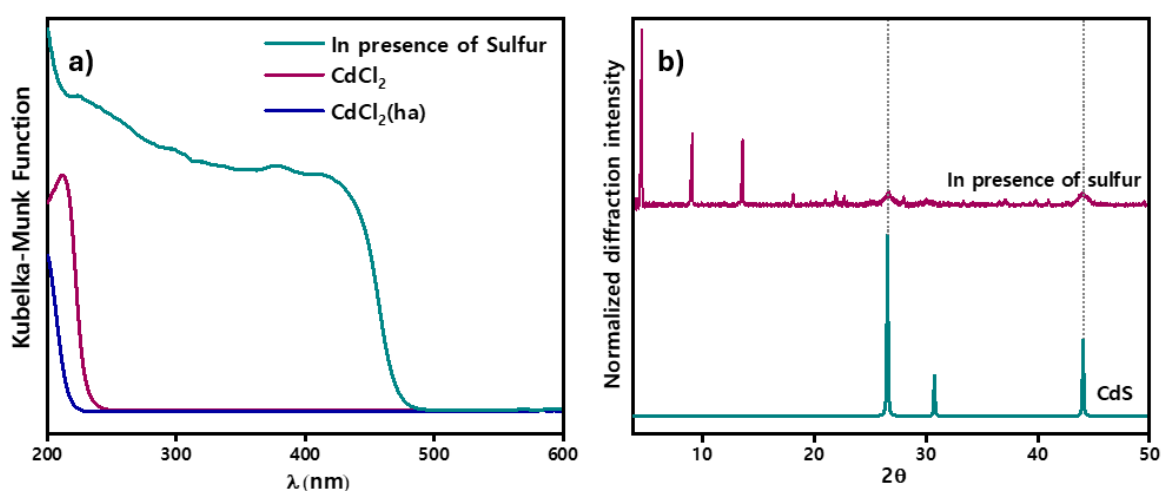


**Figure 2.4.** a) Difference in absorbance in presence and absence of sulfur and b) PXRD indicating presence of CdS nanoparticles.

The optical bandgap of the bulk CdS is about 2.4 eV. The bandgap of the material synthesized in presence of sulfur shows a bandgap of 2.64 eV, indicating discretization of energy levels and increase in bandgap owing to quantum confinement effect. So, one would expect the size of the particles in the quantum confinement regime comparable to the 2.8 nm Bohr excitonic radius of Cadmium sulfide.

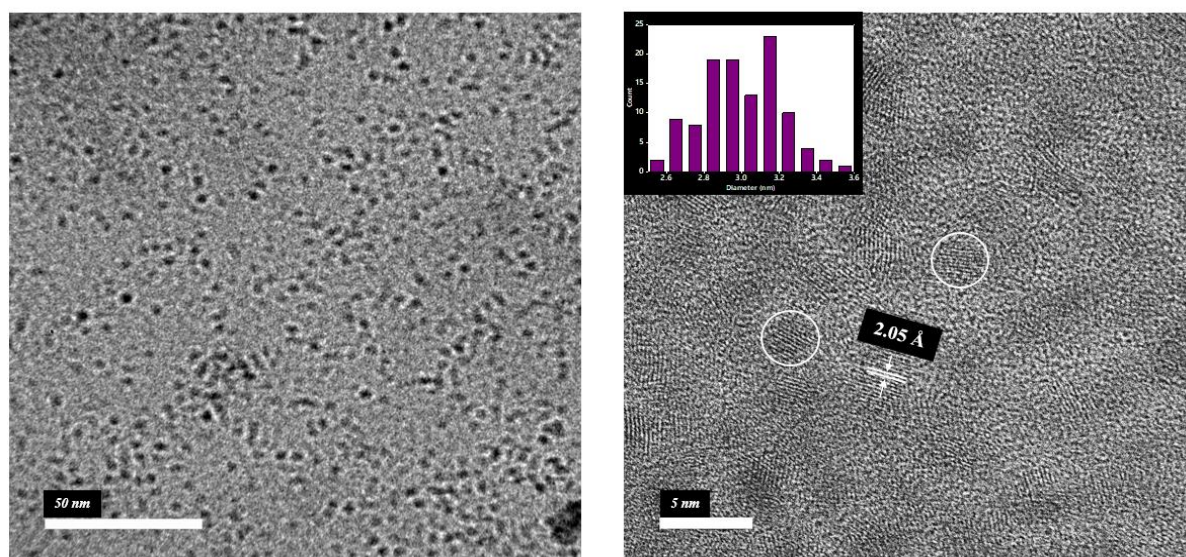


**Figure 2.5.** HRTEM analysis of CdS nanoparticles.

To confirm the presence of CdS nanoparticles, HRTEM imaging was done and particles of average size  $\sim 3$  nm were observed (Figure 2.5). Moreover, we see lattice fringes of d-spacing  $2.05 \pm 0.12$  Å, and the diffraction peak corresponding to this plane (220) appears at  $\sim 43.03^\circ$  in the PXRD pattern. This serves as further proof for the formation of CdS nanoparticles.

In conclusion, structural studies suggest that a mixture of products (i) CdS nanoparticles and (ii) Cadmium Chloride (hexylamine) layered hybrid compound are formed in synthesis. We proceed to study the optical properties to possibly gain insights to characterize the material.

The optical absorption and emission properties of a semiconductor are a result of electron-photon interactions. The interactions are described by scattering theory through absorption and emission of a quanta of light (i.e., photon). While both intraband and interband processes are usually possible in semiconductors, the interband scattering involving valence band and conduction band has more significance in terms of device applications.<sup>25</sup>

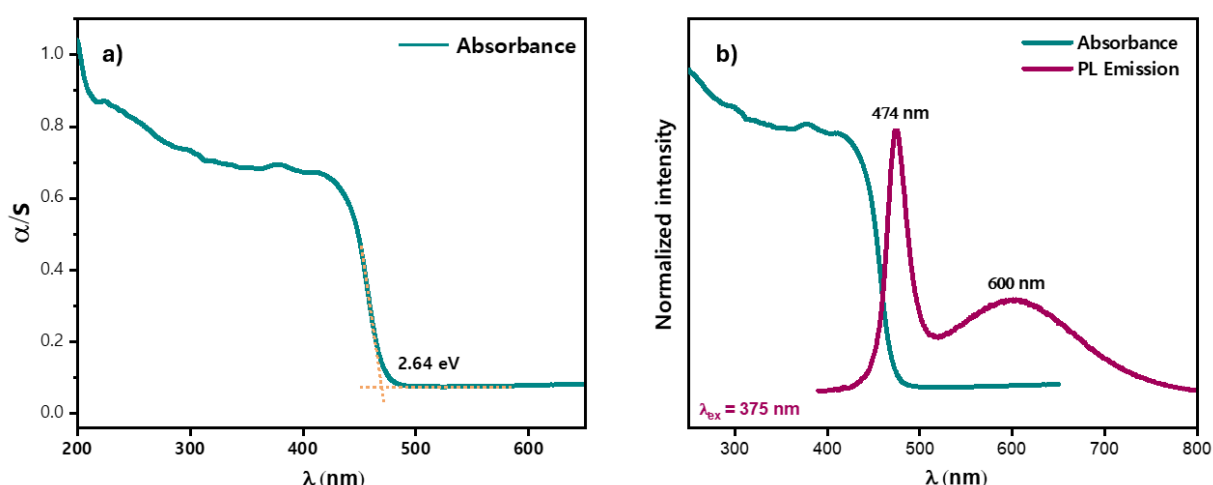


**Figure 2.6. a)** Absorption spectra showing optical bandgap of 2.64 eV **b)** Photoluminescence spectra on excitation with 375 nm laser.

The absorbance (Figure 2.6a) shows a sharp rise at 469 nm indicating an optical bandgap of 2.64 eV, which suggests the presence of quantum confinement effect considering the bandgap of bulk CdS (2.4 eV). Further increase in absorption intensity at energies above bandgap signifies the presence of a continuum of energy states in the conduction band, characteristic of a semiconducting material.

The photoluminescence spectrum (Figure 2.6b) shows two peaks, a broad peak centred at 600 nm and another relatively narrow peak at 474 nm. The higher energy peak corresponds to the band-edge emission and the broader lower energy peak possibly originates from a lattice defect state in the mid-gap range. Considering the low Stokes shift from excitonic absorption, the narrow FWHM of 0.22eV, and the average luminescence lifetime of 3 nanoseconds (Figure 2.7a), it appears logical to conclude that the origin of this higher energy emission is the presence of excitons. This gives us a preliminary idea about the structure of our synthesized sample. For the discretization of energy states and exciton formation, it is necessary

that the size of the semiconductor is comparable or less than the Bohr excitonic radius. But in case of hybrid semiconductors, this is achieved through use of organic spacers with very low dielectric constant acting as potential barriers, in sharp contrast to the semiconducting layer which acts as a potential well owing to high dielectric constant. This dielectric mismatch results in the phenomenon of dielectric confinement and gives rise to exciton formation.<sup>26</sup>

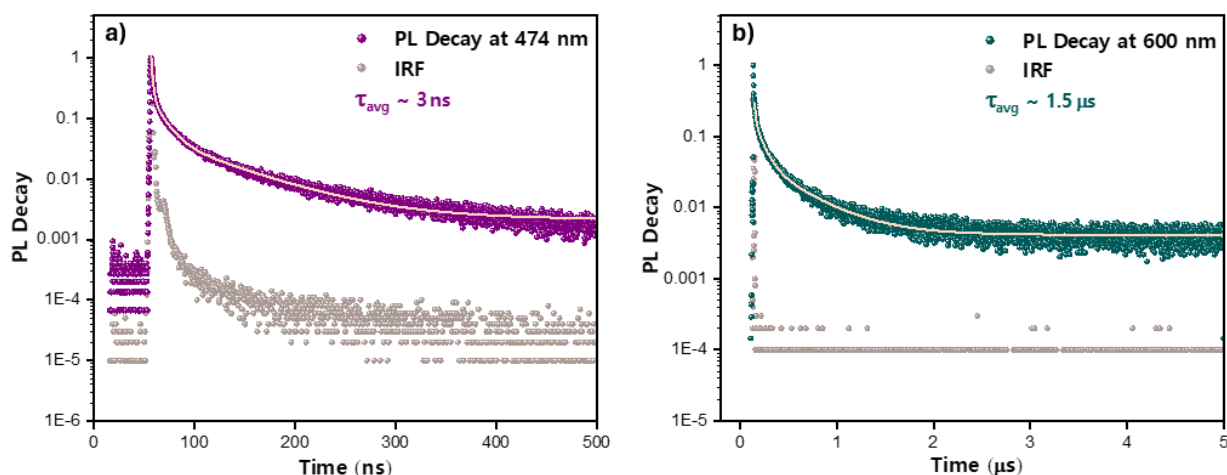


**Figure 2.7.** a) Photoluminescence decay of 474 nm peak shown along with Instrument Response Function (IRF) b) Photoluminescence decay of 600 nm peak shown along with IRF ( $\lambda_{ex} = 375$  nm laser)

The average lifetime of the higher energy peak at 474 nm is calculated from triexponential decay fit to be about 3 nanoseconds, which agrees with typical values reported in literature for excitonic emission in semiconductors. The lower energy emission has a much higher average lifetime of 1.5 microseconds (Figure 2.7b). In addition, The maxima of the broad peak and the FWHM of 0.53eV indicates that it is possibly a deep trap state with energy difference of 0.58 eV from the band-edge energy.

Temperature dependent photoluminescence measurements were done to further investigate the origin of the two emission peaks and to possibly reveal structural changes like crystal phase transitions if present. It is observed that (Figure 2.8) with decrease in temperature from room temperature to 7K, the integrated photoluminescence intensity increases systematically. The overall increase is almost close to an order of magnitude, and it is attributed to reduced exciton-phonon coupling in cryogenic-temperatures resulting in decrease of non-radiative decay channels.



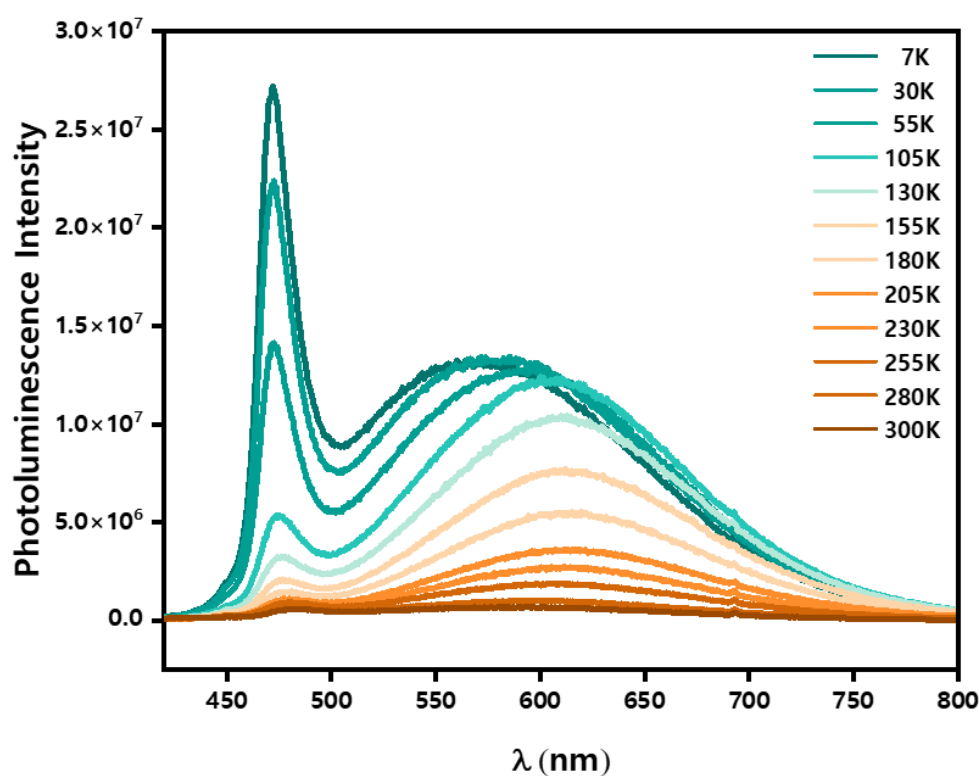


**Figure 2.8.** Photoluminescence spectra measured at different temperatures between 300K to 7K

It is not surprising that the overall luminescence intensity of a crystalline material increases at lower temperatures. However, it is of interest to resolve the contributions of the two emission peaks in the temperature range.

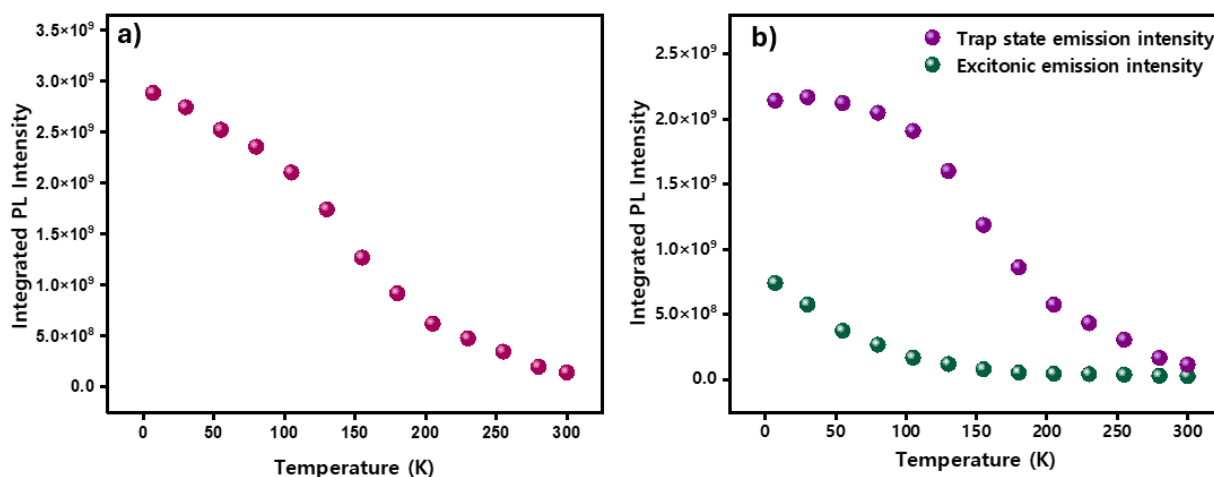


**Figure 2.9.** a) Plot showing systematic increase in integrated photoluminescence intensity with decrease in temperature b) Contributions of the excitonic and trap state emission to overall integrated intensity.

Figure 2.9a shows the trend in change of total integrated luminescence intensity with temperature. Further, it is evident on deconvolution of the two peaks that the trap state emission is the major contributor in overall emission profile (Figure 2.9b), especially at lower temperatures. The lifetime of PL decay of this broad peak ( $\lambda_{\text{max}} = 600 \text{ nm}$ ) is observed to increase progressively 300K to cryo-temperatures (Figure 2.10). This could again be attributed to the suppression of non-radiative channels of decay, more of which are activated with increasing temperature. Especially in case of hybrid semiconductors comprising of organic spacers in their crystal structure, the effect of lattice vibrations and the resulting exciton-phonon coupling on luminescence intensity and lifetimes is significant.

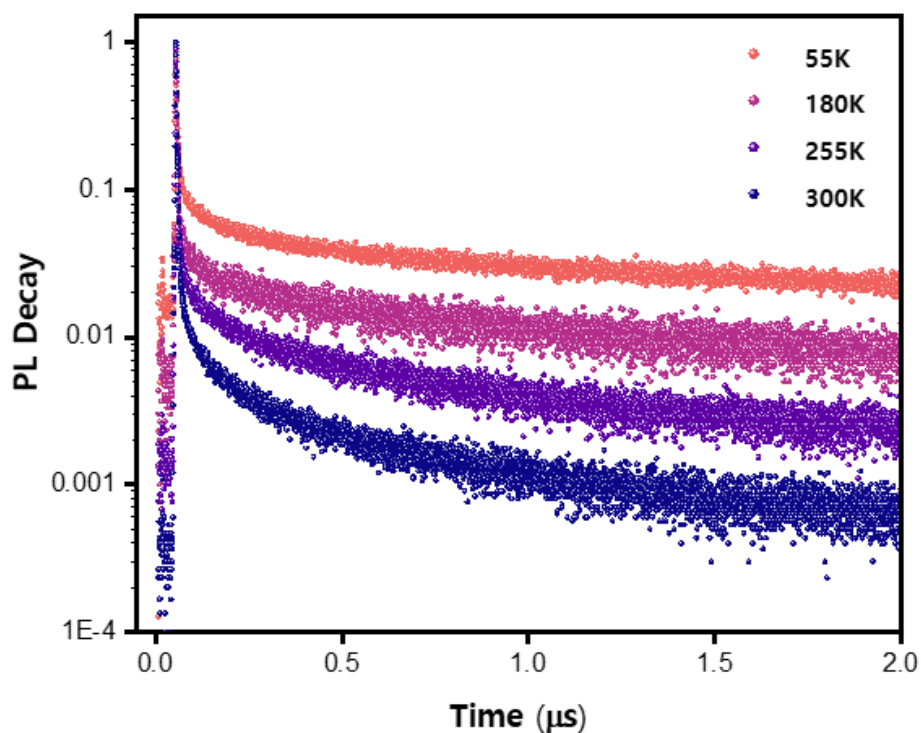


**Figure 2.10.** Increase in photoluminescence decay lifetimes at lower temperatures due to reduced number of non-radiative channels.

Although the contribution of the higher energy excitonic emission is lesser, it is essential to take a closer look at the change in contribution with temperature (2.11a) doing which might potentially reveal information about the nature of the trap as well as the excitonic state.



Moreover, investigating the change in FWHM of the excitonic emission might also provide information on the extent of spectral broadening due to thermally activated exciton-phonon interactions in such semiconductors. The trend in temperature-dependence of FWHM of the excitonic emission is not a monotonous function of temperature, rather it shows an anomalous behavior (Figure 2.11b), inverting at about 180K.

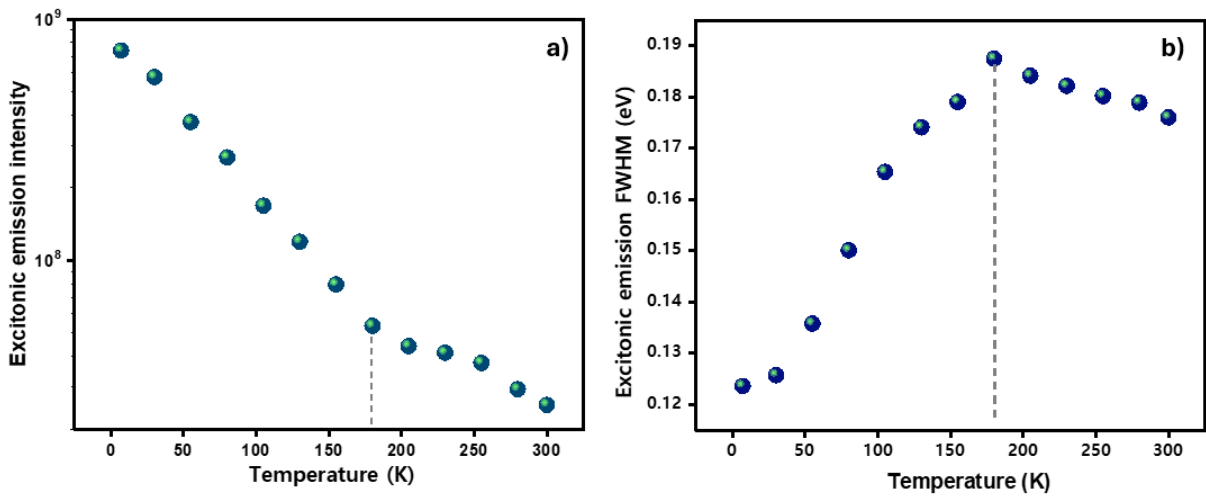


**Figure 2.11.** a) Plot showing logarithmic increase in excitonic intensity with reducing temperature b) Temperature dependence of FWHM of excitonic emission.

If it was solely the temperature-dependent exciton—acoustic-phonon and exciton—optical-phonon interactions influencing the FWHM of the excitonic peak, one would expect an increase in the exciton linewidth in accordance to the equation<sup>27</sup> relating the broadening parameter ( $\gamma$ ) with temperature:

$$\Gamma = \Gamma_0 + |A_1|T + |A_2|/(e^{\hbar\Omega_0/kT} - 1)$$

But we observe an initial increasing behavior which flips at 180K to progressively decrease till room temperature. At the same point, we also observe a change of slope in the plot  $\log(I)$  vs.  $T$ , where  $I$  is the excitonic emission intensity. So, it appears that there are more complex processes occurring in this temperature range.

Further, the energy shift with temperature also appears to flip behavior in the same temperature range. An overall blue shift in excitonic emission is observed due to bandgap increase as explained by Varshni in 1967 (Figure 2.12a).<sup>28</sup> But a deviation seems to exist at temperatures around 180K. Similarly, the decrease in energy of STE emission maxima abruptly inverts the behavior precisely at that range to show increase energy of emission maxima (Figure 2.12b) thereafter.

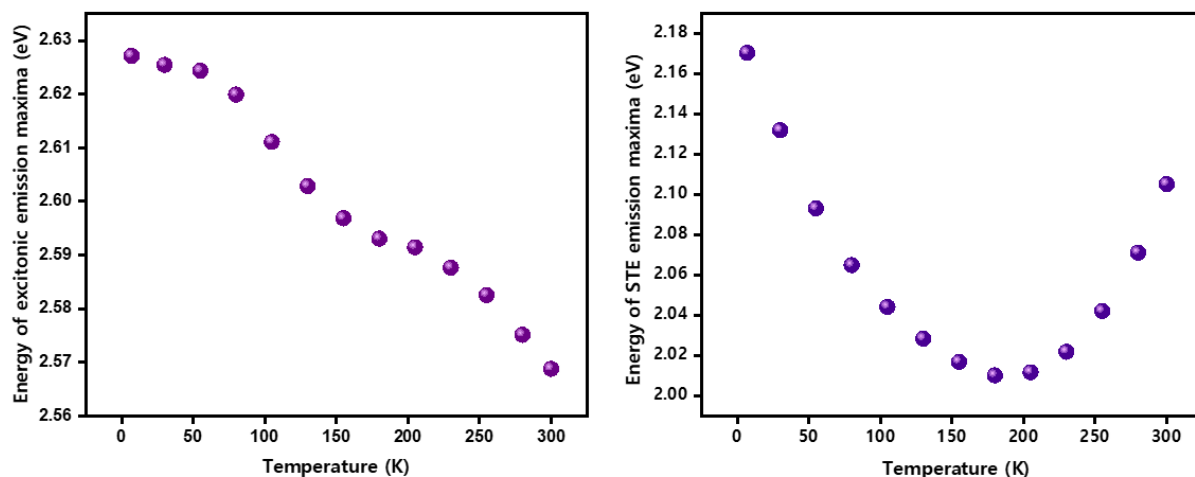


**Figure 2.12.** a) Blue shift in excitonic emission maxima with lowering temperature showing deviation around 180K. b) Energy shift of STE emission maxima inverting behavior at 180K

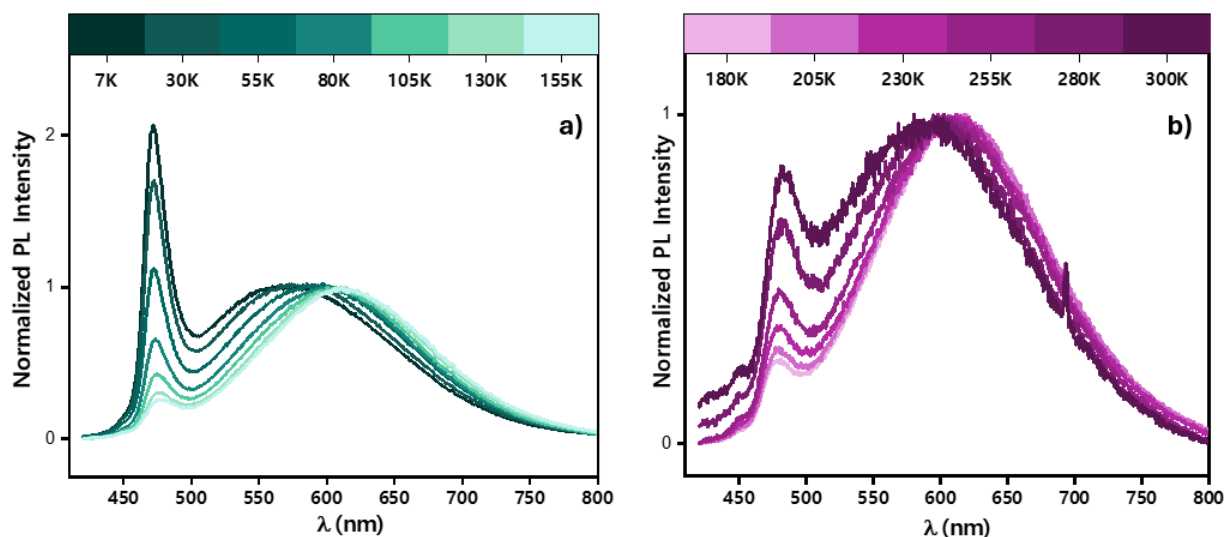


**Figure 2.13.** a) Decrease in excitonic emission intensity relative to broad emission band from 7K to 155K. b) Relative intensity of excitonic emission increasing with respect to broad emission band from 180K to room temperature.

To decipher why the specific trends are observed in energy of emission maxima, excitonic FWHM, emission intensity etc. and find the mechanism behind this behavior, we specifically study the trends in relative intensities of the two emission bands. The influence of overall intensity increase can be nullified by normalizing the spectra at the emission maxima of one of the peaks as shown (Figure 2.13a, 2.13b).

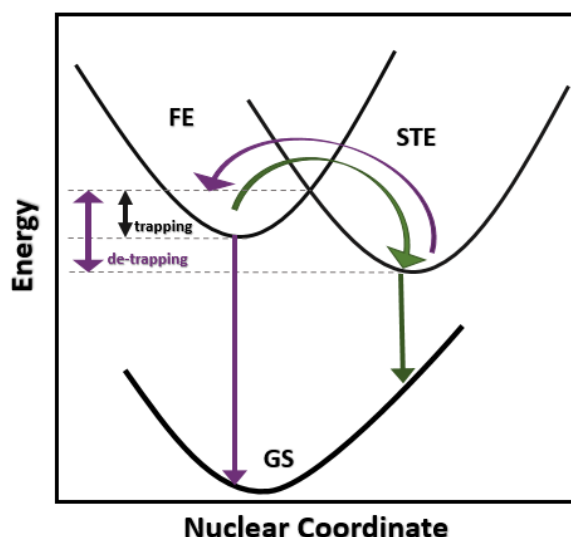


**Figure 2.14.** Schematic showing exciton trapping and de-trapping mechanism indicating difference in energy barrier between the two processes

On doing so, we observe a systematic decrease in excitonic emission with increasing temperature initially which possibly represents the exciton trapping process being favoured as a result of thermally-induced lattice vibrations.<sup>29</sup> On further increase in thermal energy beyond 180K, the exciton de-trapping process appears to be favoured once the system is provided with energy to cross the higher energy barrier involved in the de-trapping process.<sup>30</sup> Figure 2.14 shows the trapping-detraping process and indicates the different energy barriers between the two processes.

The objective of this work was to synthesize the 2D hybrid semiconductor –  $\text{Cd}_2\text{S}_2(\text{hexylamine})$  and investigate the temperature-dependence of luminescent properties. However, through structural and optical studies, we found that a mixture of two compounds were formed i) a new type of cadmium halide based hybrid compound and ii) CdS nanocrystals, which is the origin of the photoluminescence properties. We further observed exciton-trapping and de-trapping processes in the CdS nanoparticles. We conclude that the compound  $\text{Cd}_2\text{S}_2(\text{hexylamine})$  was not synthesized, and further novel strategies might be employed to synthesize cadmium chalcogenide based hybrid class of materials. However, one can try exploring the variation in properties with change in halide composition in this new type of transition-metal hybrid halide material synthesized.

## Bibliography

---

1. Pelant, I. & Valenta, J. *Luminescence Spectroscopy of Semiconductors*. (Oxford university press, Oxford, 2012).
2. Liu, M. *et al.* Colloidal quantum dot electronics. *Nat. Electron.* **4**, 548–558 (2021).
3. Han, T. *et al.* *Photoelectric Materials and Devices*. (WORLD SCIENTIFIC, 2021). doi:10.1142/12109.
4. Morita, Y., Yoshioka, K. & Kuwata-Gonokami, M. Observation of Bose-Einstein condensates of excitons in a bulk semiconductor. *Nat. Commun.* **13**, 5388 (2022).
5. Murray, C. B., Norris, D. J. & Bawendi, M. G. Synthesis and characterization of nearly monodisperse CdE (E = sulfur, selenium, tellurium) semiconductor nanocrystallites. *J. Am. Chem. Soc.* **115**, 8706–8715 (1993).
6. Ekimov, A. I. & Onushchenko, A. A. Quantum Size Effect in Three-Dimensional Microscopic Semiconductor Crystals. *JETP Lett.* **118**, S15–S17 (2023).
7. Cotta, M. A. Quantum Dots and Their Applications: What Lies Ahead? *ACS Appl. Nano Mater.* **3**, 4920–4924 (2020).
8. Triana, M. A., Hsiang, E.-L., Zhang, C., Dong, Y. & Wu, S.-T. Luminescent Nanomaterials for Energy-Efficient Display and Healthcare. *ACS Energy Lett.* **7**, 1001–1020 (2022).
9. Ye, T. *et al.* II–VI Organic–Inorganic Hybrid Nanostructures with Greatly Enhanced Optoelectronic Properties, Perfectly Ordered Structures, and Shelf Stability of Over 15 Years. *ACS Nano* **15**, 10565–10576 (2021).
10. Li, X., Hoffman, J. M. & Kanatzidis, M. G. The 2D Halide Perovskite Rulebook: How the Spacer Influences Everything from the Structure to Optoelectronic Device Efficiency. *Chem. Rev.* **121**, 2230–2291 (2021).
11. Naaman, R. & Waldeck, D. H. Chiral-Induced Spin Selectivity Effect. *J. Phys. Chem. Lett.* **3**, 2178–2187 (2012).

- 
12. Long, G. *et al.* Chiral-perovskite optoelectronics. *Nat. Rev. Mater.* **5**, 423–439 (2020).
  13. Rebilly, J.-N., Gardner, P. W., Darling, G. R., Bacsá, J. & Rosseinsky, M. J. Chiral II–VI Semiconductor Nanostructure Superlattices Based on an Amino Acid Ligand. *Inorg. Chem.* **47**, 9390–9399 (2008).
  14. Huang, X., Li, J. & Fu, H. The First Covalent Organic–Inorganic Networks of Hybrid Chalcogenides: Structures That May Lead to a New Type of Quantum Wells. *J. Am. Chem. Soc.* **122**, 8789–8790 (2000).
  15. Huang, X., Li, J., Zhang, Y. & Mascarenhas, A. From 1D Chain to 3D Network: Tuning Hybrid II-VI Nanostructures and Their Optical Properties. *J. Am. Chem. Soc.* **125**, 7049–7055 (2003).
  16. Huang, X. & Li, J. From Single to Multiple Atomic Layers: A Unique Approach to the Systematic Tuning of Structures and Properties of Inorganic–Organic Hybrid Nanostructured Semiconductors. *J. Am. Chem. Soc.* **129**, 3157–3162 (2007).
  17. Roushan, M., Zhang, X. & Li, J. Solution-Processable White-Light-Emitting Hybrid Semiconductor Bulk Materials with High Photoluminescence Quantum Efficiency. *Angew. Chem. Int. Ed.* **51**, 436–439 (2012).
  18. Yao, W. & Yu, S. Synthesis of Semiconducting Functional Materials in Solution: From II-VI Semiconductor to Inorganic–Organic Hybrid Semiconductor Nanomaterials. *Adv. Funct. Mater.* **18**, 3357–3366 (2008).
  19. Ki, W. & Li, J. A Semiconductor Bulk Material That Emits Direct White Light. *J. Am. Chem. Soc.* **130**, 8114–8115 (2008).
  20. Ki, W., Li, J., Eda, G. & Chhowalla, M. Direct white light emission from inorganic–organic hybrid semiconductor bulk materials. *J. Mater. Chem.* **20**, 10676 (2010).

- 
21. Fang, X. *et al.* Tuning and Enhancing White Light Emission of II–VI Based Inorganic–Organic Hybrid Semiconductors as Single-Phased Phosphors. *Chem. Mater.* **24**, 1710–1717 (2012).
  22. Wei, S., Lu, J. & Qian, Y. Density Functional Study of 2D Semiconductor CdSe·*hda*<sub>0.5</sub> (*hda* = 1,6-hexanediamine) and Its Excitonic Optical Properties. *Chem. Mater.* **20**, 7220–7227 (2008).
  23. Wang, S. & Li, J. Two-dimensional inorganic–organic hybrid semiconductors composed of double-layered ZnS and monoamines with aromatic and heterocyclic aliphatic rings: Syntheses, structures, and properties. *J. Solid State Chem.* **224**, 40–44 (2015).
  24. Huang, X. *et al.* Flexible Hybrid Semiconductors with Low Thermal Conductivity: The Role of Organic Diamines. *Angew. Chem. Int. Ed.* **48**, 7871–7874 (2009).
  25. Singh, J. *Electronic and Optoelectronic Properties of Semiconductor Structures*. (Cambridge University Press, 2003).  
doi:10.1017/CBO9780511805745.
  26. Chakraborty, R. & Nag, A. Dielectric confinement for designing compositions and optoelectronic properties of 2D layered hybrid perovskites. *Phys. Chem. Chem. Phys.* **23**, 82–93 (2021).
  27. Abay, B., Efeoğlu, H. & Yoğurtçu, Y. K. Low-temperature photoluminescence of n-InSe layer semiconductor crystals. *Mater. Res. Bull.* **33**, 1401–1410 (1998).
  28. Varshni, Y. P. Temperature dependence of the energy gap in semiconductors. *Physica* **34**, 149–154 (1967).
  29. Smith, M. D. & Karunadasa, H. I. White-Light Emission from Layered Halide Perovskites. *Acc. Chem. Res.* **51**, 619–627 (2018).
  30. Tang, L. *et al.* Temperature-Dependent Photoluminescence of CdS/ZnS Core/Shell Quantum Dots for Temperature Sensors. *Sensors* **22**, 8993 (2022).